Supplementary Materials for

Circadian Rhythm of Redox State Regulates Excitability in Suprachiasmatic Nucleus Neurons

Tongfei A. Wang, Yanxun V. Yu, Gubbi Govindaiah, Xiaoying Ye, Liana Artinian, Todd P. Coleman, Jonathan V. Sweedler, Charles L. Cox, Martha U. Gillette *

*To whom correspondence should be addressed. E-mail: mgillett@illinois.edu

This PDF file includes:

Materials and Methods
Supplementary Text
Figs. S1 to S6
References

Materials and Methods

Animals and brain slice preparation

   LE/BluGill rats (University of Illinois) were used for real-time imaging of redox state measurement, BioGEE assay, DHA/AA assay, and patch-clamp recording; they were maintained under a 12:12 hour light/dark (L/D) schedule, receiving food and water *ad libitum*. C57BL6 mice from Jackson Laboratory (Bar Harbor, ME) were used for real-time imaging of redox state, maintained under a 12:12 hour L/D schedule, receiving food and water *ad libitum*. *Bmal 1* +/- heterozygotes were obtained from Jackson Laboratory (Bar Harbor, ME), and homozygous *Bmal 1 -/-* were bred from the heterozygotes. *Bmal1 -/-* mice were maintained under a 12:12 hour L/D schedule, receiving food and water *ad libitum*, until 3 d before experiments, when they were moved to dark/dark (D/D), receiving food and water *ad libitum (29)*. All protocols were approved by the IACUC at University of Illinois, Urbana-Champaign, and fully compliant with NIH guidelines for humane treatment of animals.

   Organotypic brain slice cultures were prepared from 3-4-wk-old animals, sacrificed between ZT 5-7. A 400-μm-thick coronal hypothalamic brain slice containing the paired SCN was cut on mechanical chopper, then transferred to a Millipore tissue culture insert (Millipore, Billerica, MA) with DMEM containing 0.5% B27 supplement, 1.0 mM glutamine and 25 µg/ml penicillin/streptomycin (Gibco, Carlsbad, CA). Organotypic slices were fed the next day and ready for imaging after 2 d *in vitro* (DIV).

   Animals for BioGEE and DHA/AA assays were 5-7-wk old. A 500-μm-thick coronal hypothalamic brain slice containing the paired SCN was cut on mechanical chopper between ZT 2-10, depending on the experimental time to be examined. Some samples were duration-matched to control for time *in vitro*. The SCN was punched with a 2 mm-diameter corer, to remove non-SCN tissues. These reduced brain slices were maintained in the brain slice chamber, perfused with Earle's Essential Balanced Salt Solution (EBSS, NaCl 116.4 mM, KCl 5.4 mM, $CaCl_2$ 1.8 mM, $MgSO_4$ 0.8 mM, NaH_2PO_4 1.0 mM, glucose 24.5 mM, $NaHCO_3$ 26.2 mM, gentamicin 1.0 mg/L, pH 7.3, 300 mOsm/L) saturated with 95% O_2/5% CO_2 at 37°C for at least 2 h until collection for biochemical assay at specific CTs.

   Animals for patch-clamp studies were 2-wk old, and sacrificed from ZT 2-10, depending on the experimental time to be examined. The brain was quickly removed and placed into cold, oxygenated slicing medium: KCl 2.5 mM, $MgSO_4$ 10.0 mM, $CaCl_2$ 0.5 mM, NaH_2PO_4 1.2 mM, $NaHCO_3$ 26.0 mM, glucose 11.0 mM, and sucrose 234.0 mM, saturated with 95% O_2/5% CO_2. A 350-μm-thick brain slice containing paired SCN was cut using a vibrating blade microtome (Leica, Wetzlar, DE). Brain slices were then transferred to a holding chamber containing artificial cerebrospinal fluid (ACSF): NaCl 126.0 mM, KCl 2.5 mM, $CaCl_2$ 2.0 mM, $MgCl_2$, 2.0 mM, NaH_2PO_4 1.2 mM, glucose 10.0 mM, $NaHCO_3$ 26.0 mM, 300 mOsm/L, saturated with 95% O_2/5% CO_2 at room temperature. Brain slices were incubated at least 1 h before recording commenced.

Real-time redox imaging (long-term)

An organotypic slice cultured for 2 DIV was transferred to a 37 °C chamber on the microscope stage, where EBSS was perfused continuously. Two-photon laser-scanning microscopy was performed with the Zeiss LSM 510 confocal laser-scanning microscope system equipped with MaiTai laser and 20X 0.8 N.A. objective (Carl Zeiss, Obercochen, DE). Excitation wavelength was 730 nm, while 2 channels of emission at 430-500 nm and 500-550 nm were recorded simultaneously *(30)*. Tissue was examined up to 15 μm from the surface. Imaging started at CT 10 and frame-scan, with sampling rate at 4 sec/frame plus 356-sec interval, was performed for 720 frames (72 h total). Fluorescence intensity of series scanning at 400+ and 500+ nm for each frame was acquired by Zeiss LSM software (function of region of interest, ROI). Relative redox state was calculated from the ratio of fluorescence at 500+ over 400+ (F_{500+}/F_{400+}).

χ^2 periodogram was performed with a MATLAB toolbox, ClockLab (Actimetrics, Wilmette, IL), to quantify the length of circadian period (τ). χ^2 values were calculated from recording data from WT rat, WT mouse, and KO mouse, and the τ was determined from the highest value above confidence interval of 0.001. Recording datasets with no χ^2 values above 0.001 confidence interval, or with calculated $\tau > 32$ h, which is the mathematical consequence of estimating a period that is approximately half of the length of the recording time, were not regarded as circadian.

Real-time redox imaging (short-term)

An organotypic slice cultured for 2 DIV was incubated in EBSS for at least 2 h before transferred to microscope stage, with the same set-up as above. A frame-scan, with sampling rate at 4 sec/frame plus 26-sec interval, was performed for 60 frames (30 min total). Redox reagents (diamide, DIA, 5 mM or glutathione, GSH, 1 mM, Sigma, St. Louis, MO) were delivered through a syringe pump from 5 – 15 min. Fluorescence intensity of series scanning at 400+ and 500+ nm for each frame was acquired by Zeiss LSM software. Relative redox state was calculated from the ratio of fluorescence at 500+ over 400+ (F_{500+}/F_{400+}). Redox changes before and during drug treatment were based on the average ratio of F_{500+}/F_{400+} between 1-2 min *vs.* 15-16 min, respectively.

BioGEE assay

Reduced SCN brain slices *(31)* were incubated with 250 μM biotinylated glutathione ethyl ester (BioGEE, Invitrogen, Carlsbad, CA) for 1 h *(32)* at CT 0-1, 6-7, 11-12, 13-14, or 19-20. After freezing by dry ice, tissue was stored at -80 °C until assay. Frozen tissue samples were mixed with 30 μL Tissue Protein Extraction Reagent (T-PER, Pierce, Rockford, IL), plus 0.2% SDS, 1 mM EDTA, and 1x Complete protease inhibitor cocktail (CalBioChem, Darmstadt, DE) on ice, and homogenized. After 2-min incubation on ice, the samples were centrifuged at 14,000 rmp for 2 min, and the supernatant was transferred to a clean tube. Protein content of each sample was determined by BCA protein assay (Pierce, Rockford, IL). Total protein (25 μg/sample) was resolved in 8% SDS-PAGE and transferred to nitrocellulose membrane (Bio-Rad, Hercules, CA). Membranes were probed with 1:2,000 dilution of mouse anti-biotin-peroxidase antibody (Cellsignaling, Danvers, MA) overnight, and developed with SuperSignal West Femto Maximum Sensitivity Substrate (Pierce, Rockford, IL). After scanning, the anti-

biotin antibody was stripped by Restore Western Blot Stripping Buffer (Thermo, Rockford, IL), and an anti-tubulin antibody (Cellsignaling, Danvers, MA) was applied to probe total tubulin level. After incubation with secondary antibody, the membrane was developed with SuperSignal Pico Chemiluminescent Substrate (Thermo, Rockford, IL), and scanned again. The relative glutathiolation level was determined by the ratio of overall biotin intensity of each lane over the band intensity of tubulin, and then normalized to the maximum value on the same gel. One-Way ANOVA was used for statistical analysis, followed by Tukey Honestly Significant Difference (HSD) Test for multiple comparisons.

DHA/AA assay

Reduced SCN brain slices were collected at CT 4, 8, 14, 20, and 23 in pre-chilled microtubes on dry ice. Each slice was homogenized with 50 μL acetate buffer, and further centrifuged at 10,000 rmp at 4 °C for 5 min; two aliquots (2.5 μL each) of supernatant were sampled for DHA or DHA+AA concentration, respectively. For DHA derivatization, the sample was mixed with 1.5 μL of 1 mg/mL 4,5-dimethyl-1,2-phenylenediamine (DMPD) solution in phosphate buffer; after 4-min incubation at room temperature, an extra 1 μL of phosphate buffer was added to bring the final volume to 5 μL. DHA+AA concentration was obtained with similar procedure, except for adding 1 μL of 17 units of ascorbate oxidase (Roche, Basel, CH) solution and reacting for 1 min before derivatization, to oxidize AA to DHA. DHA or DHA+AA were measured by capillary electrophoresis with laser-induced fluorescence (CE-LIF) detection using DMPD *(33)*. Peak heights in standards and samples were determined by Grams 386 software (Thermo Galactic, Salem, NH), and sample concentration was determined by linear regression; the ratio of DHA/AA was calculated to evaluate the relative redox state in SCN tissue. One-Way ANOVA was used for statistical analysis, followed by Tukey HSD Test for multiple comparisons.

Patch-clamp recording

Whole-cell patch electrodes had pipette-tip resistances of 4-6 MΩ, and were filled with a solution containing: K-gluconate 140.0 mM, KCl 5.0 mM, CaCl$_2$ 0.07 mM, MgCl$_2$ 1.0 mM, EGTA 0.1 mM, HEPES 10.0 mM, Na-ATP 4.0 mM, Na-GTP 0.4 mM, pH 7.3, and osmolality 290-300 mOsm/L. Recordings were performed using a Multiclamp 700B amplifier (Molecular Devices, Sunnyvale, CA). Signals were sampled at 10 kHz, low-pass filtered at 10 kHz using a Digidata 1320 digitizer, and stored on computer for subsequent analyses using pClamp software (Molecular Devices, Sunnyvale, CA).

Membrane potential (V_m) of SCN neurons was recorded under current-clamp mode, 2 min/cell. A total of 364 SCN neurons were recorded at different CTs, with running means calculated over 24 h. In addition, average V_m at 5 CTs (CT 1, 7, 11, 14, and 20) were calculated. One-Way ANOVA was performed for statistical analysis, followed by Tukey HSD Test for multiple comparisons.

Input resistance (R_{in}) of SCN neurons was recorded from the same population as for V_m above. During recording, a current injection of -20 pA every 17 s was applied to test membrane potential changes, and R_{in} were determined from the changes of V_m over

testing current ($R_{in} = \Delta V / -20$ pA). A sub-population of the current-clamped SCN neurons were challenged with a current-steps protocol (duration 800 ms) from -100 pA to 120 pA, with a 20 pA increment at CTs 1, 7, 11, 14, and 20, to construct the current-voltage (I-V) curve and precisely calculate R_{in}. In this case, R_{in} was determined from the slope of the I-V curve at 0 pA holding current by linear regression. One-Way ANOVA was performed for statistical analysis, followed by Tukey HSD Test for multiple comparisons.

Membrane properties, including V_m, R_{in}, and spontaneous action potential (SAP) frequency, of neurons discharging SAP during the 2-min recording (active neurons) *vs.* the inactive group (no SAP detected during the 2-min recording) were further examined at CT 7 and CT 14. Student's *t*-Test was performed for statistical analysis.

Some of the current-clamped SCN neurons were treated with redox reagents (DIA or GSH) and responses were examined at specific CTs. The initial V_m was recorded immediately after whole-cell clamp, and then a current-steps protocol was performed to construct the current-voltage (I-V) curve at rest. Next, redox reagents were bath-applied and ΔV_m was recorded. Before wash-out, another current-steps protocol was performed so that the I-V curve under drug treatment was obtained. To prevent secondary effects from synaptic transmission, TTX (1μM, Tocris, Ellisville, MO), a voltage-gated Na^+ channel blocker, was applied during the entire process.

Changes of membrane potential (ΔV_m) in response to redox reagents were compared by paired Student's *t*-Test. ΔV_m was further classified by CT and averaged. One-Way ANOVA followed by the Tukey HSD Test was performed for statistical analysis. Redox reagent-induced changes in the I-V curve and R_{in} were compared by paired Student's *t*-Test. Percentage changes of R_{in} were further calculated and classified by CT. Averaged data were subjected to One-Way ANOVA.

Recording electrode containing the redox reagents (DIA or GSH) was used in current-clamp recording to determine the action site of redox regulation. The electrode was front-filled with normal intracellular solution, and back-filled with drug-containing solution. Immediately after whole-cell clamp, the shifting V_m was recorded for 5 min. The ΔV_m was determined from the difference between the V_m plateau at the end and the initial V_m at the start. Changes of V_m in response to redox reagents were subjected to paired Student's *t*-Test.

Under voltage-clamp mode, a slow ramp of voltage from -50 mV to -110 mV and back to -50 mV was applied to SCN neurons, 6 s/trial, 3 trials/min. During this process, redox reagents were bath-perfused and the holding currents changes were recorded. Inhibitors of voltage-gated Na^+ channels (TTX, 1μM), AMPA-Rs (DNQX, 20 μM, Tocris, Ellisville, MO) and NMDA-Rs (d-CPP, 10 μM, Tocris, Ellisville, MO) were applied during the entire process. Holding current was plotted against the command voltage so that I-V curves before and during treatments were obtained. DIA-evoked currents were calculated based on the difference between the two I-V curves. To further test the hypothesis that K^+ channel(s) is a target of redox regulation, Cs^+ (140 mM) was used as an alternative of K^+-filled glass electrode. Difference between control and DIA treatment

on the holding current and conductance changes were determined from the first 100 pixels of the ramp from -50 mV, and analyzed by paired Student's t-Test. Similar recordings and analysis were performed with reducing reagent, GSH, and with K^+ electrodes in the presence of bupavacaine (Bupi, 100 µM, Tocris, Ellisville, MO), a leak K^+-channel blocker. One-Way ANOVA followed by the Tukey HSD Test was performed for statistical analysis.

The voltage-step command recording was performed in ACSF with HEPES buffer: NaCl 138.0 mM (118.0 mM, in the presence of TEA), KCl 2.5 mM, $CaCl_2$ 2.0 mM, $MgCl_2$, 2.0 mM, glucose 10.0 mM, HEPES 10.0 mM, pH 7.3, 300 mOsm/L, saturated with 100% O_2 at 37 ℃. Voltage-clamped SCN neurons were held at -60 mV, and challenged with -10 mV pulses (250 ms duration) twice with an interval of 3 s; a 400 ms pre-pulse of -90 mV then -40 mV was delivered before each pulse. A cocktail of inhibitors of voltage-gated Na^+ channels (TTX, 1 µM), Ca^{2+} channels (Cd^{2+}, 200 µM), AMPA-Rs (DNQX, 20 µM), NMDA-Rs (d-CPP, 10 µM) and $GABA_A$-Rs (SR95531, 10 µM, Tocris, Ellisville, MO) was applied in ACSF during the entire process; in addition, 10 mM EGTA was included in the recording electrode solution to block Ca^{2+}_i fluctuation. Each sweep was repeated every 20 s, before, during and after treatment with redox reagent (DIA and GSH), as well as K^+ channels inhibitors (4-aminopyridine, 4-AP, 5 mM; tetraethylammonium, TEA, 20 mM, Sigma, St. Louis, MO) treatment. Voltage-dependent K^+ current in response to -10 mV voltage-step stimulation was calculated from the difference between the current responses to the voltage-step command of -10 mV steps, following either -90 mV or -40 mV pre-pulse. The transient peak current within 10 ms and the persistent current between 230 – 250 ms were analyzed across the treatments of redox reagents (DIA, GSH) and K^+ channels blockers (4-AP, TEA). One-Way ANOVA followed by the Tukey HSD Test was performed for statistical analysis.

Supplementary Text

Ratiometric Redox Fluorometry
Only oxidized FAD and reduced NAD(P)H exhibit intrinsic fluorescence, and these two signals respond oppositely to changes in redox state; thus, ratiometric redox fluorometry based on FAD and NAD(P)H can be used to evaluate cellular metabolism. This strategy is suitable for long-term imaging, because it minimizes fluctuations of interfering factors, such as light absorption of excitation and emission, light scattering, and mitochondrial density

Circadian Oscillation of Membrane Excitability in SCN Neurons
During subjective midday (CT 7), SCN neuronal activity was maximal: resting V_m was relatively depolarized (-55.17 ± 0.61 mV), with higher R_{in} (816.6 ± 58.7 MΩ), SAP frequency (1.65 Hz, mean of active and inactive cells), and percentage of active cells (neurons discharging SAP during the period of recording, 57.8%). During subjective night, these parameters were significantly lower: V_m was hyperpolarized (Fig. 2B, minimum at CT 14, -60.15 ± 0.69 mV), with decreased R_{in} (Fig. 2D, CT 14, 583.7 ± 32.0 MΩ), SAP frequency (CT 13, 0.55 Hz), and active-cell percentage (CT 16, 20.8%). These

results match to the pattern of daily changing SAP frequency detected by single-unit activity recording in rat SCN slice (Fig. S2B). Further analysis with the active *vs.* inactive neurons at CT 7 and CT 14 illustrates a more robust oscillation occurring in active neurons than inactive ones (Fig. S3, $P < 0.05$, Student's *t*-Test; $n = 22$-31).
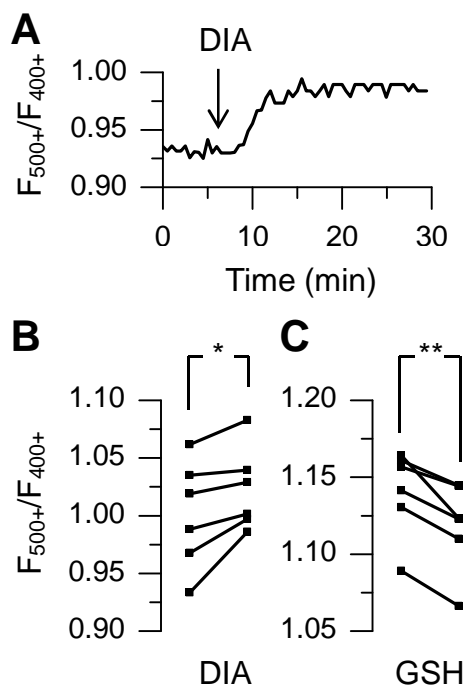
Supplementary Figures

Fig. S1. Real-time changes in SCN redox state in response to exposure to redox reagents. **(A)** Sample trace of real-time redox imaging of SCN slice, during application of the oxidizing reagent, DIA (5 mM, 5 - 15 min). DIA induces an increase of the ratio of F_{500+}/F_{400+} in < 2 min, indicating a shift toward oxidized state. **(B)** Summary of the effect of DIA treatment, which shifts the SCN towards oxidized state; each line represents an individual slice trial (*, $P < 0.05$, paired Student's t-Test; $N = 6$). **(C)** Summary of the effect of GSH treatment, which shifts the SCN towards reduced state; each line represent an individual slice trial (**, $P < 0.01$, paired Student's t-Test; $N = 6$). Amplitudes of these redox reagent-induced shifts are comparable to the amplitude of the endogenous redox oscillation (Fig. 1).
.
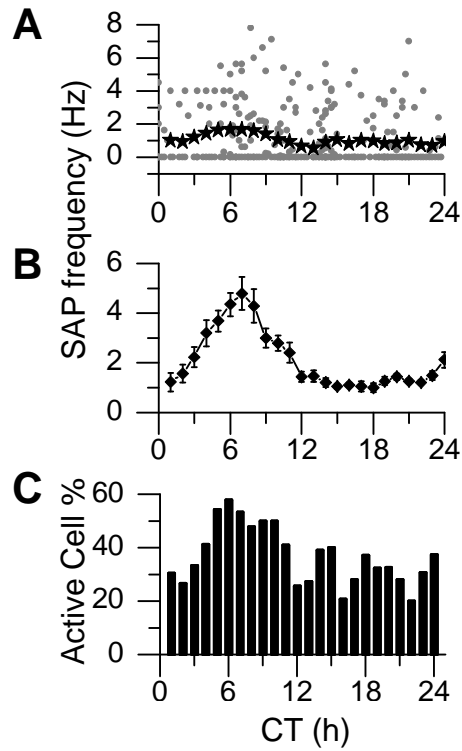
Fig. S2. Circadian rhythm of spontaneous action potentials (SAP) in rat SCN neurons. **(A)** SAP frequencies were recorded from current-clamped SCN neurons (grey dot = SAP frequency of each individual neuron, $N = 334$; black star = averaged SAP frequency in each hour). **(B)** SAP frequencies peak near midday (single-unit activity recorded extracellularly). **(C)** Percentage of neurons discharging SAP per 2-min recording, plotted in each hour over the circadian cycle.
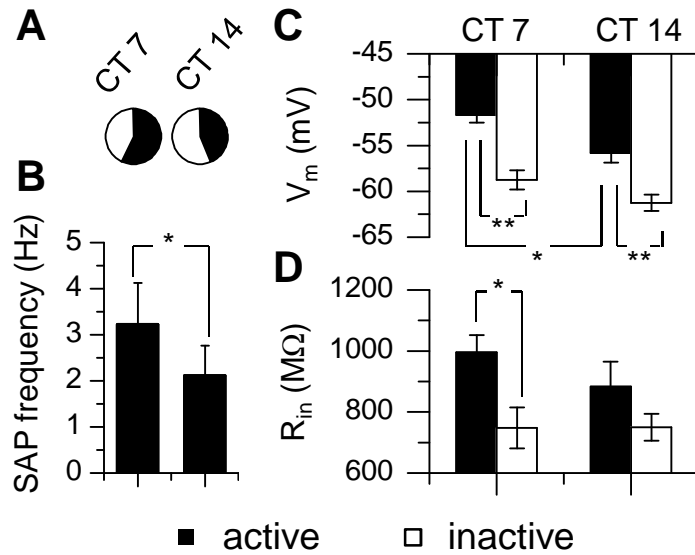
Fig. S3. Membrane properties of active *vs* inactive SCN neurons at CT 7 and CT 14 (active neurons was defined as neurons discharging SAP during the 2-min recording, while the inactive ones were those without detected SAP). **(A)** 2-min recording detected more active neurons at CT 7 (active : inactive = 29 : 22) than CT 14 (active : inactive = 24 : 31). **(B)** Average SAP frequence of active neurons were higher at CT 7 than CT 14 (*, $P < 0.05$, Student's *t*-Test; $N = 24$-29). **(C)** V_m of active neurons was more depolarized than inactive neurons at both CT 7 and CT 14 (**, $P < 0.01$, Student's *t*-Test; $N = 22$-31); in addition, the active neurons at CT 7 were more depolarized than CT 14, while the V_m of inactive neurons remained unchanged (*, $P < 0.05$, Student's *t*-Test; $N = 24$-29). **(D)** R_{in} of active neurons was higher than inactive neurons at CT 7, but not at CT 14 (*, $P < 0.05$, Student's *t*-Test; $N = 22$-31).

.
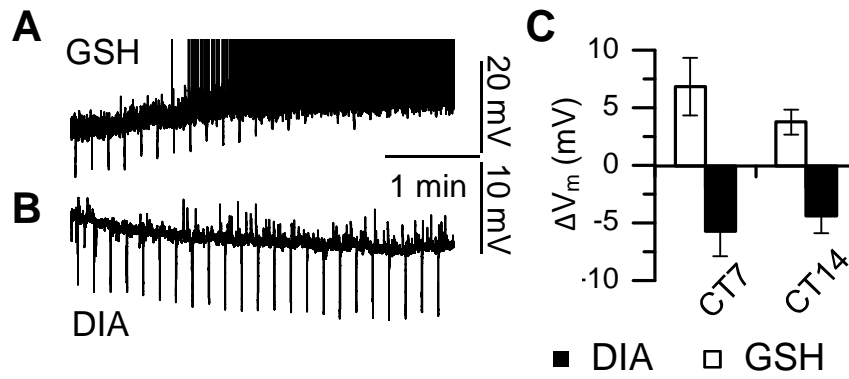
Fig. S4. Current-clamp recording of V_m from SCN neurons with patch pipettes containing redox reagents at CT 7 and CT 14. **(A, B)** Representative voltage traces showing the changes in membrane potential in GSH (A) and DIA (B) electrode. **(C)** Summary of V_m shift at CT 7 and CT 14 ($P < 0.01$, paired Student's t-Test to control; $N = 5$-6).
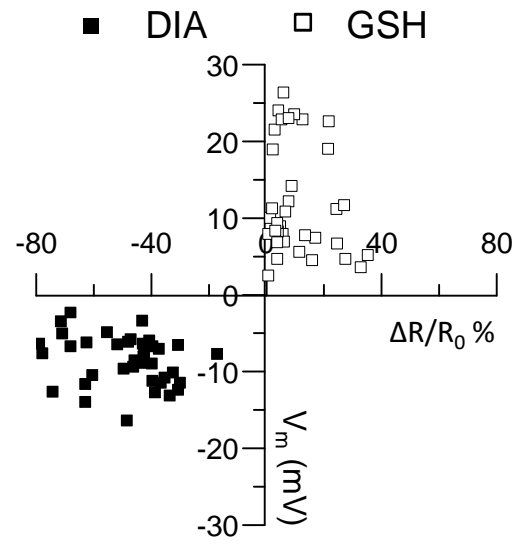
.

Fig. S5. Changes of V_m induced by redox reagents (DIA, filled; GSH, open) were independent from the changes of R_{in} ($P > 0.05$, Linear Correlation and Regression; $N = 37\text{-}41$).

.

Transcriptional-Translational Oscillator

Redox Oscillator

(A)

(B) **(C)**

Membrane Excitability Oscillation
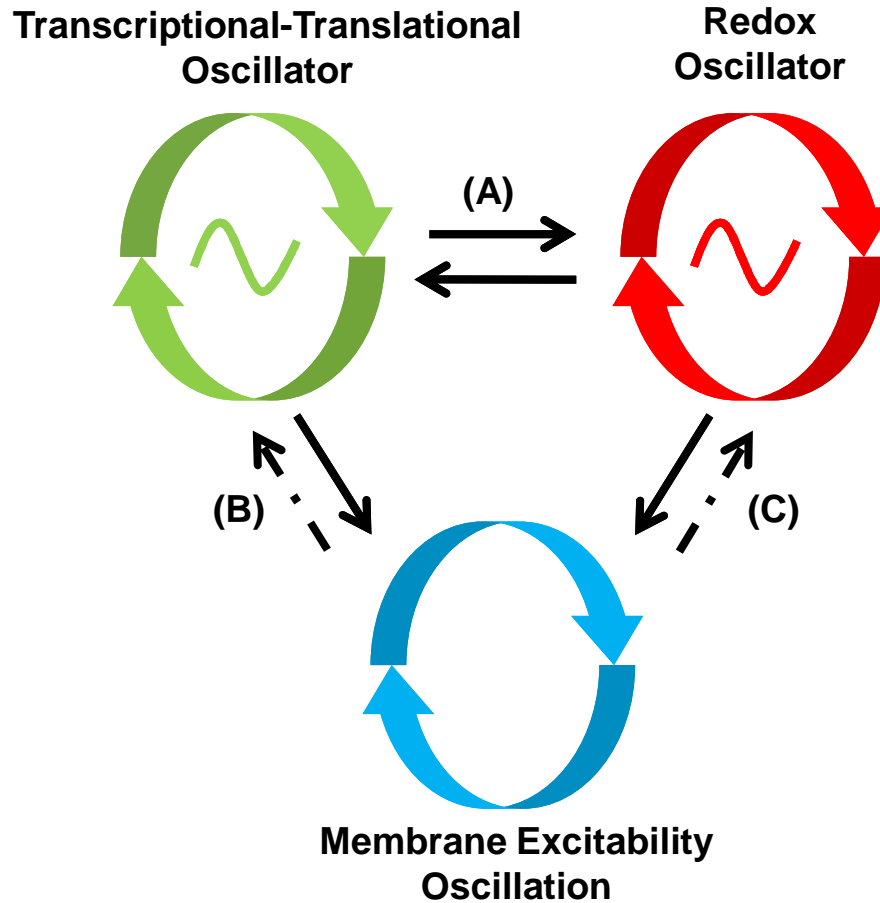
Fig. S6. Proposed model of the relative interdependency of the transcriptional-translational oscillator, redox oscillator, and membrane excitability oscillation. **(A)** The circadian oscillation of redox state in SCN depends upon functionally intact transcriptional-translational machinery (Fig. 1), *(34)*, and redox state modulates clock-genes expression, reciprocally (solid arrows) *(35-38)*. **(B)** Several ion channels, which underlie membrane excitability, are rhythmically expressed under the control of clock genes (solid arrow) *(39)*; conversely, membrane excitability in SCN neurons can gate signal input to the transcriptional-translational oscillator, which in turn affects clock-gene expression (dashed arrow) *(40-43)*. **(C)** Redox state can regulate neuronal excitability in SCN neurons via K^+ currents (solid arrow) (Fig. 2 through 4); concomitantly, increased neuronal activity can increase blood flow, glucose uptake by astrocytes, and energy availability, which can feedback to modulate neuronal metabolic state (dashed arrow) *(44)*.

.

References

1. C. B. Green, J. S. Takahashi, J. Bass, The meter of metabolism. *Cell* **134**, 728 (2008). doi:10.1016/j.cell.2008.08.022 Medline

2. J. Bass, J. S. Takahashi, Circadian integration of metabolism and energetics. *Science* **330**, 1349 (2010). doi:10.1126/science.1195027 Medline

3. P. L. Lowrey, J. S. Takahashi, Mammalian circadian biology: Elucidating genome-wide levels of temporal organization. *Annu. Rev. Genomics Hum. Genet.* **5**, 407 (2004). doi:10.1146/annurev.genom.5.061903.175925 Medline

4. R. A. Prosser, M. U. Gillette, Cyclic changes in cAMP concentration and phosphodiesterase activity in a mammalian circadian clock studied in vitro. *Brain Res.* **568**, 185 (1991). doi:10.1016/0006-8993(91)91396-I Medline

5. J. S. O'Neill, E. S. Maywood, J. E. Chesham, J. S. Takahashi, M. H. Hastings, cAMP-dependent signaling as a core component of the mammalian circadian pacemaker. *Science* **320**, 949 (2008). doi:10.1126/science.1152506 Medline

6. M. C. Harrisingh, Y. Wu, G. A. Lnenicka, M. N. Nitabach, Intracellular Ca2+ regulates free-running circadian clock oscillation in vivo. *J. Neurosci.* **27**, 12489 (2007). doi:10.1523/JNEUROSCI.3680-07.2007 Medline

7. M. S. Robles, C. Boyault, D. Knutti, K. Padmanabhan, C. J. Weitz, Identification of RACK1 and protein kinase Calpha as integral components of the mammalian circadian clock. *Science* **327**, 463 (2010). doi:10.1126/science.1180067 Medline

8. W. Dröge, Free radicals in the physiological control of cell function. *Physiol. Rev.* **82**, 47 (2002). Medline

9. F. W. Turek *et al.*, Obesity and metabolic syndrome in circadian Clock mutant mice. *Science* **308**, 1043 (2005). doi:10.1126/science.1108750 Medline

10. B. Marcheva *et al.*, Disruption of the clock components CLOCK and BMAL1 leads to hypoinsulinaemia and diabetes. *Nature* **466**, 627 (2010). doi:10.1038/nature09253 Medline

11. J. Rutter, M. Reick, L. C. Wu, S. L. McKnight, Regulation of clock and NPAS2 DNA binding by the redox state of NAD cofactors. *Science* **293**, 510 (2001). doi:10.1126/science.1060698 Medline

12. E. M. Dioum *et al.*, NPAS2: A gas-responsive transcription factor. *Science* **298**, 2385 (2002). doi:10.1126/science.1078456 Medline

13. J. Rutter, M. Reick, S. L. McKnight, Metabolism and the control of circadian rhythms. *Annu. Rev. Biochem.* **71**, 307 (2002). doi:10.1146/annurev.biochem.71.090501.142857 Medline

14. S. Huang, A. A. Heikal, W. W. Webb, Two-photon fluorescence spectroscopy and microscopy of NAD(P)H and flavoprotein. *Biophys. J.* **82**, 2811 (2002). doi:10.1016/S0006-3495(02)75621-X Medline

15. Materials and methods, supplementary text, and supplementary figures are available as supplementary materials on *Science* Online.

16. M. K. Bunger *et al.*, Mop3 is an essential component of the master circadian pacemaker in mammals. *Cell* **103**, 1009 (2000). doi:10.1016/S0092-8674(00)00205-1 Medline

17. C. H. Ko *et al*., Emergence of noise-induced oscillations in the central circadian pacemaker. *PLoS Biol.* **8**, e1000513 (2010). doi:10.1371/journal.pbio.1000513 Medline

18. D. M. Sullivan, R. L. Levine, T. Finkel, Detection and affinity purification of oxidant-sensitive proteins using biotinylated glutathione ethyl ester. *Methods Enzymol.* **353**, 101 (2002). doi:10.1016/S0076-6879(02)53040-8 Medline

19. M. E. Rice, Ascorbate regulation and its neuroprotective role in the brain. *Trends Neurosci.* **23**, 209 (2000). doi:10.1016/S0166-2236(99)01543-X Medline

20. W. S. Kim, R. L. Dahlgren, L. L. Moroz, J. V. Sweedler, Ascorbic acid assays of individual neurons and neuronal tissues using capillary electrophoresis with laser-induced fluorescence detection. *Anal. Chem.* **74**, 5614 (2002). doi:10.1021/ac025917q Medline

21. J. S. O'Neill, A. B. Reddy, Circadian clocks in human red blood cells. *Nature* **469**, 498 (2011). doi:10.1038/nature09702 Medline

22. J. S. O'Neill *et al*., Circadian rhythms persist without transcription in a eukaryote. *Nature* **469**, 554 (2011). doi:10.1038/nature09654 Medline

23. M. D. Belle, C. O. Diekman, D. B. Forger, H. D. Piggins, Daily electrical silencing in the mammalian circadian clock. *Science* **326**, 281 (2009). doi:10.1126/science.1169657 Medline

24. T. M. Brown, H. D. Piggins, Electrophysiology of the suprachiasmatic circadian clock. *Prog. Neurobiol.* **82**, 229 (2007). doi:10.1016/j.pneurobio.2007.05.002 Medline

25. D. A. Golombek, R. E. Rosenstein, Physiology of circadian entrainment. *Physiol. Rev.* **90**, 1063 (2010). doi:10.1152/physrev.00009.2009 Medline

26. J. N. Itri, S. Michel, M. J. Vansteensel, J. H. Meijer, C. S. Colwell, Fast delayed rectifier potassium current is required for circadian neural activity. *Nat. Neurosci.* **8**, 650 (2005). doi:10.1038/nn1448 Medline

27. M. De Jeu, A. Geurtsen, C. Pennartz, A Ba(2+)-sensitive K(+) current contributes to the resting membrane potential of neurons in rat suprachiasmatic nucleus. *J. Neurophysiol.* **88**, 869 (2002). Medline

28. J. N. Itri *et al*., Circadian regulation of a-type potassium currents in the suprachiasmatic nucleus. *J. Neurophysiol.* **103**, 632 (2010). doi:10.1152/jn.00670.2009 Medline

29. M. K. Bunger *et al*., Mop3 is an essential component of the master circadian pacemaker in mammals. *Cell* **103**, 1009 (2000). doi:10.1016/S0092-8674(00)00205-1 Medline

30. S. Huang, A. A. Heikal, W. W. Webb, Two-photon fluorescence spectroscopy and microscopy of NAD(P)H and flavoprotein. *Biophys. J.* **82**, 2811 (2002). doi:10.1016/S0006-3495(02)75621-X Medline

31. M. U. Gillette, "SCN electrophysiology in vitro: Rhythmic activity and endogenous clock properties," in *Suprachiasmatic Nucleus: The Mind's Clock*, D. C. Klein, R. Y. Moore, S. M. Reppert, Eds. (Oxford University Press, New York, 1991), pp. 125–143.

32. D. M. Sullivan, R. L. Levine, T. Finkel, Detection and affinity purification of oxidant-sensitive proteins using biotinylated glutathione ethyl ester. *Methods Enzymol.* **353**, 101 (2002). doi:10.1016/S0076-6879(02)53040-8 Medline

33. W. S. Kim, R. L. Dahlgren, L. L. Moroz, J. V. Sweedler, Ascorbic acid assays of individual neurons and neuronal tissues using capillary electrophoresis with laser-induced fluorescence detection. *Anal. Chem.* **74**, 5614 (2002). doi:10.1021/ac025917q Medline

34. J. S. O'Neill, A. B. Reddy, Circadian clocks in human red blood cells. *Nature* **469**, 498 (2011). Medline

35. J. Rutter, M. Reick, L. C. Wu, S. L. McKnight, Regulation of clock and NPAS2 DNA binding by the redox state of NAD cofactors. *Science* **293**, 510 (2001). doi:10.1126/science.1060698 Medline

36. E. M. Dioum *et al.*, NPAS2: A gas-responsive transcription factor. *Science* **298**, 2385 (2002). doi:10.1126/science.1078456 Medline

37. A. Balsalobre, F. Damiola, U. Schibler, A serum shock induces circadian gene expression in mammalian tissue culture cells. *Cell* **93**, 929 (1998). doi:10.1016/S0092-8674(00)81199-X Medline

38. N. Preitner *et al.*, The orphan nuclear receptor REV-ERBalpha controls circadian transcription within the positive limb of the mammalian circadian oscillator. *Cell* **110**, 251 (2002). doi:10.1016/S0092-8674(02)00825-5 Medline

39. T. M. Brown, H. D. Piggins, Electrophysiology of the suprachiasmatic circadian clock. *Prog. Neurobiol.* **82**, 229 (2007). doi:10.1016/j.pneurobio.2007.05.002 Medline

40. M. U. Gillette, J. W. Mitchell, Signaling in the suprachiasmatic nucleus: Selectively responsive and integrative. *Cell Tissue Res.* **309**, 99 (2002). doi:10.1007/s00441-002-0576-1 Medline

41. D. A. Golombek, R. E. Rosenstein, Physiology of circadian entrainment. *Physiol. Rev.* **90**, 1063 (2010). doi:10.1152/physrev.00009.2009 Medline

42. M. N. Nitabach, J. Blau, T. C. Holmes, Electrical silencing of *Drosophila* pacemaker neurons stops the free-running circadian clock. *Cell* **109**, 485 (2002). doi:10.1016/S0092-8674(02)00737-7 Medline

43. G. B. Lundkvist, Y. Kwak, E. K. Davis, H. Tei, G. D. Block, A calcium flux is required for circadian rhythm generation in mammalian pacemaker neurons. *J. Neurosci.* **25**, 7682 (2005). doi:10.1523/JNEUROSCI.2211-05.2005 Medline

44. J. Rutter, M. Reick, S. L. McKnight, Metabolism and the control of circadian rhythms. *Annu. Rev. Biochem.* **71**, 307 (2002). doi:10.1146/annurev.biochem.71.090501.142857 Medline